Backus Spencer ORCID iD: 0000-0002-6466-053X

Design and Testing of the JPL-Nautilus Gripper for Deep-Ocean Geological Sampling

Spencer B Backus
NASA Jet Propulsion Laboratory
4800 Oak Grove Drive
Pasadena, CA 91109
spencer.backus@jpl.nasa.gov

Rina Onishi
Stanford University
Stanford, CA 94305
ronishi@stanford.edu

Andrew Bocklund
Virginia Tech
Blacksburg, VA 24061
andrewb98@vt.edu

Andrew Berg
NASA Jet Propulsion Laboratory
4800 Oak Grove Drive
Pasadena, CA 91109
Andrew.B.Berg@jpl.nasa.gov

Eric D Contreras
NASA Jet Propulsion Laboratory
4800 Oak Grove Drive
Pasadena, CA 91109
eric.d.contreras@jpl.nasa.gov

Aaron Parness
NASA Jet Propulsion Laboratory
4800 Oak Grove Drive
Pasadena, CA 91109
aaron.parness@jpl.nasa.gov

Abstract

We present the design and experimental results for the JPL-Nautilus Gripper, a 16-finger highly-underactuated microspine gripper for use in the deep ocean. The gripper can grasp objects from 10 to 30 cm in size and anchor to flat and curved rocky surfaces (i.e. cliff faces and sea mounts). Laboratory results demonstrated an anchoring capability of greater than 450 N on rough rocks in both shear and normal loading directions. Deployment on the Hercules ROV (Remotely Operated Vehicle) aboard the E/V Nautilus on three deep-ocean dives verified performance at depths up to to 2100

This is the author manuscript accepted for publication and has undergone full peer review but has not been through the copyediting, typesetting, pagination and proofreading process, which may lead to differences between this version and the Version of Record. Please cite this article as doi: 10.1002/rob.21934

meters with approximately 100 N loads applied through the ROV's thrusters, including moment loads. The gripper also serves as a development unit for future robotic tools that will include a coring drill in the center of the gripper, as previously demonstrated in non-ocean environments with microspine grippers. Such a tool will facilitate the collection of geologic samples from the deep ocean using more agile and cost-effective systems.

1 Introduction

Collecting representative rock samples is central to any geological expedition but the lack of appropriate sampling tools limits the collection of sea-floor samples to specimens that can be picked up off the sea-floor or broken off from outcrops. Currently, most marine drill based sampling systems consist of dedicated drill ships or large multi-ton dedicated robotic drills capable of taking core samples that are 10s to 100s of meters long [Sager et al., 2003]. There are a few remotely operated underwater vehicle (ROV) operated drill systems but these systems still take relatively large cores and can only operate when the ROV has parked on the sea-floor or thrusts against a cliff face [Stakes et al., 1997, Ludvigsen et al., 2017, Murton, 2016]. Therefore the marine geology community has repeatedly expressed a desire for a small, vehicle agnostic drill that can be handled by a robotic manipulator and collect oriented cores in a wide range of terrains and rock types from a free floating vehicle [Sager et al., 2003, German and Tominaga, 2016, Emerson and Shank, 2016, Hayman and Perfit, 2016, ROV Manipulator-Based Drilling for Deep Submergence Science, 2015]. Anchoring the drill to the target rock may be necessary to hold the vehicle in position and counteract drilling loads.

Here we present the design and evaluation of a micro-spine based rock anchor (shown in operation in Fig. 1) that may be combined with a coring drill in the future to facilitate collection of small rock cores from a free floating ROV. This design leverages prior work combining micro-spine grasping with rock drilling that has been conducted for microgravity sampling but adapts it to the marine environment [Parness, 2011, Parness and Frost, 2012, Parness et al., 2013, Parness et al., 2017b]. In the remainder of this paper we present a brief overview of existing ROV mounted drills and the work to date on microspine anchors developed for sampling, describe the design and fabrication of the JPL-Nautilus Gripper, the methods and results of lab based characterization of its capabilities, and its performance on a field trial conducted aboard the E/V Nautilus on cruise NA101 to the Papahānaumokuākea Marine National Monument.

1.1 Related Work

Very few ROV operated rock sampling drills have been developed and existing drills have all been mounted directly to the body of the vehicle. The WHOI/MBARI drill is mounts under the ROV and can take horizontally oriented, meter long cores [Stakes et al., 1997]. In contrast, the remotely operated coring system (ROCS) and National Research Council MarineE Tech drills mount to the front of the ROV and take vertically oriented cores [Ludvigsen et al., 2017, Murton, 2016, Josso, 2016]. In all three cases, the vehicle is used to position the drill and hold it in position while collecting a rock core. To

Figure 1: The JPL-Nautilus gripper, located at the end of the robotic arm, anchors the ROV Hercules to exposed rock on a seamount at 2000m depth.

do so, the ROV must land on a flat area of the sea floor (for the vertically oriented drills), or drive up against a steep/vertical cliff face (for the horizontally oriented drill), limiting where core samples can be taken in all three cases. To enable collecting samples from an arbitrarily orientated surface from a free floating vehicle, researchers have proposed a marine sampling drill that first anchors itself to the substrate using arms tipped with small self drilling anchors but as far as the authors are aware, this system has not been developed further [ROV Manipulator-Based Drilling for Deep Submergence Science, 2015].

Like free floating submersibles, vehicles in microgravity must counteract any forces arising from a sampling operation with their attitude control system or by directly anchor themselves to the body being sampled. Although collecting images and samples from a floating vehicle while actively maintaining its position has been demonstrated both on earth and for spacecraft [Greenberg et al., 2005, Sakagami et al., 2013, Backes et al., 2017], directly anchoring to the substrate being sampled and counteracting forces into it through the anchor greatly simplifies operations if sampling takes a significant amount of time as is the case when collecting rock cores. To this effect, a series of microspine based grippers that incorporated a rotary percussive drill have been developed for anchoring to and sampling asteroids in microgravity [Parness, 2011, Parness and Frost, 2012, Parness et al., 2013, Parness et al., 2017b]. These

grippers rely on microspine based adhesion, first developed for wall climbing robots [Asbeck et al., 2006, Wang et al., 2019, Carpenter et al., 2016] to anchor the vehicle to the substrate and counteract the loads from the drill that is used to collect a sample or further secure the vehicle. Lastly, related microspine based anchors have been adapted for use by divers underwater and were tested on the NASA Extreme Environment Mission Operations (NEEMO) program. This gripper was designed to be attached to the seafloor by the diver and then server as a secure handle [Parness et al., 2017a].

Various other grippers have been adapted or specifically designed for marine applications. Licht et al. present a jamming gripper capable of operating at depth that conforms to and grasps irregular objects [Licht et al., 2016]. Li et al. present a hybrid pincer and spine based gripper for grasping and sampling plating scleractinian mesophotic corals [Li et al., 2019]. The AMADEUS sub-sea hand consists of three hydraulically actuated parallel mechanism based fingers [Lane et al., 1999]. Soft robotic grippers composed of hydraulically actuated cast polymer fingers have also been adapted for marine use, particularly sampling delicate organisms [Galloway et al., 2016]. Lastly, several fully and underactuated cable driven grippers have been demonstrated [Bemfica et al., 2014, Stuart et al., 2014, Stuart et al., 2017, Mura et al., 2018]. Like the JPL-Nautilus gripper, the soft robotic grippers and underactuated hands like the Ocean One Hand have more degrees of freedom than actuated inputs and are designed to passively conform to the environment [Birglen et al., 2007]. However these grippers are designed to grasp relatively small objects and lack the JPL-Nautilus grippers ability to anchor to surfaces and counteract large loads.

2 JPL-Nautilus Gripper Design and Fabrication

The JPL-Nautilus Gripper, shown in Fig. 2, consists of 16 radially symmetric digits and all of the digits are actuated with equal force via a single input and force balancing differential. Each digit consists of a revolute joint at its base, a quasi-prismatic joint realized through a four bar linkage between the proximal and distal links, and a large metal spine at its tip. The proximal and distal joints are flexed by a single tendon and extended by an extension tendon and constant force spring respectively. Equal force is applied to each digit's flexor tendon by a continuous loop based force balancing differential. The overall gripper is both held and actuated by the parallel jaw end effector built into the robotic arm. The parallel jaw gripper grasps the T-Bar handle, and rotates it to open and close the gripper. Rotation of the gripper body is prevented by the bracing bar that contacts the arm proximal to the wrist rotation joint.

2.1 Linkage Design

The design of the linkage and selection of the particular spines used on the JPL-Nautilus Gripper were based on prior work conducted as part of the Asteroid Redirect Mission (ARM) [Parness et al., 2017b]. The ARM gripper was designed to attach the spacecraft to the surface of the asteroid and counteract the drilling loads or weight on bit (WOB, the normal force applied to the drill bit) of an undercutting anchor drill. The key driving assumption of the mission was that the surface to be

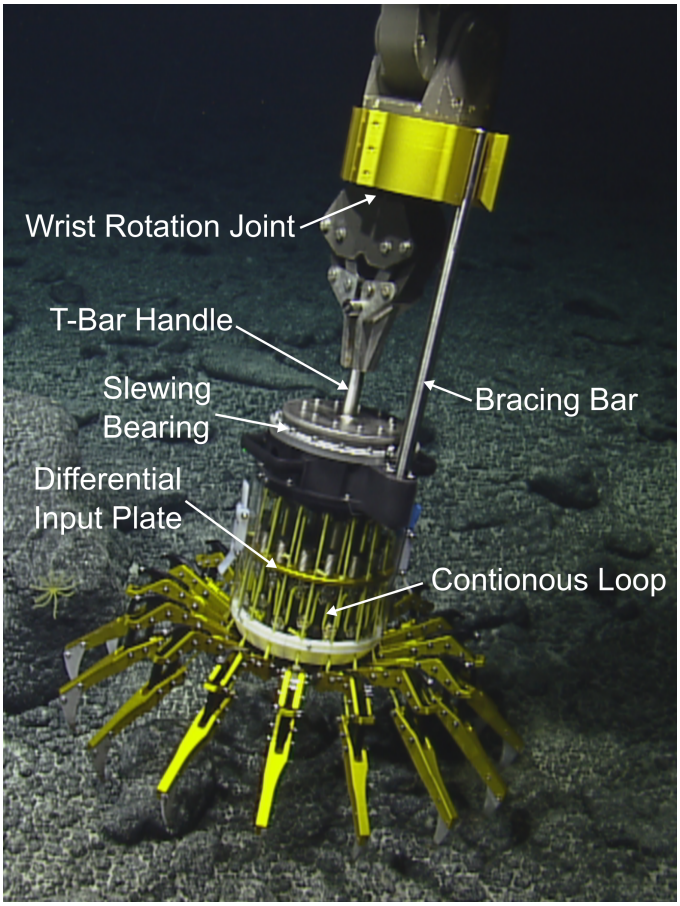

Figure 2: The JPL-Nautilus Gripper consists of 16 radially symmetric microspine fingers actuated by a single input via a force balancing differential mechanism. It is mechanically actuated by rotating the T-Handle via the wrist actuator of the robotic arm.

gripped has a bulk curvature with an equivalent diameter between 1-4m, but the surface is irregular, with variation on macro-, medium-, and micro- scales. The linkage design developed for this gripper provides conformance to a defined range of surface profiles appropriate to an asteroid surface and creates the necessary relative motion of the microspine interface to provide adhesion to the surface.

The initial linkage design, shown in Fig. 3, employed a revolute proximal joint and prismatic distal joint to engage the spines with the surface. This topology maintained a constant hook angle throughout the stroke of the prismatic joint, as desired based on previous work that showed that hook angle had an effect on grip strength [Carpenter et al., 2016, Asbeck et al., 2006]. However, the link tended to collide with intermediate obstacles, preventing the microspines from making contact with the surface. This resulted in low performance. Two other topologies were considered, referred to as crank and slider and four-bar, shown in Fig. 4. The crank and slider topology suffered from collisions with the body of the gripper in the retracted (raised) position, which limited the available stroke of the proximal joint and prevented the digits from retracting sufficiently above the palm of the gripper to allow for expected palmer misalignment with the grasp surface. This linkage topology also resulted in larger changes in

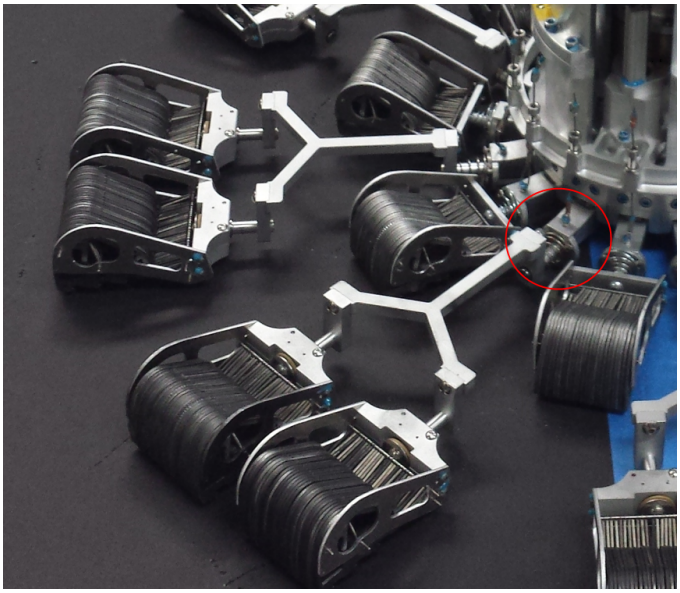

Figure 3: The initial ARM gripper prototype used a revolute-prismatic joint (circled in red) that allowed each digit to swing down to conform to the surface and then translate in to engage the spines.

hook angle throughout its stroke and provided inconsistent and near-zero adhesion force. In contrast, the four-bar design provides near constant hook angle over its strokes so the hook angle can be set near an optimum ($\approx 45°$) for a given material and be expected to be close to this value at any point in the stroke. In testing, the four-bar mechanism produced good adhesion on a variety of materials, so it was selected.

Once a topology was selected, fine tuning of the pivot height, mechanism travel, and spring parameters were assessed empirically. One early realization was that longer linkages develop more WOB for a given surface curvature because the preload of the hooks directly drives the tool into the surface. That is, more of the shear force imparted by the hooks is counteracted by tool to surface contact as opposed to being counteracted by hooks on the opposite side of the circular array.

Next, the effects of the pivot height, mechanism travel, and spring parameters were explored using the same test apparatus mentioned above. The WOB achieved was then compared to find a region in the parameter space where sufficient WOB was achieved over a range of parameter values. This ensured that the gripper would be tolerant to off-nominal conditions. This method produced the final linkage show in Fig. 5 that achieves acceptable grip on a wide variety of gripping surfaces in spite of the high variability in measured WOB that is produced by testing on natural rock materials.

Lastly, several different hook configurations were tested: small hooks (size 6), medium hooks (size 3/0), large hooks (size 5/0), and a single extra large hook (referred to as megalodon). As shown in Fig. 6, the single large megalodon hook outperformed the arrays of smaller hooks for soft materials with a compressive strengths of 700kPa and 2MPa. When engaging on softer materials, the single large hook was observed to dig into the material like a plow, resulting in good performance. In contrast, for hard

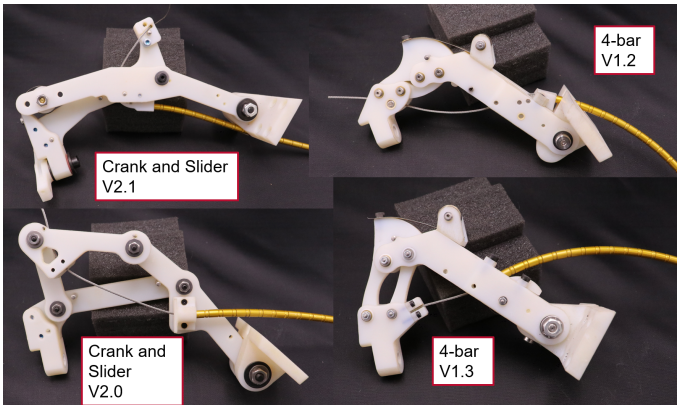

Figure 4: Prototypes of other linkage topologies that were explored including the crank and slider and four-bar linkages are shown here.

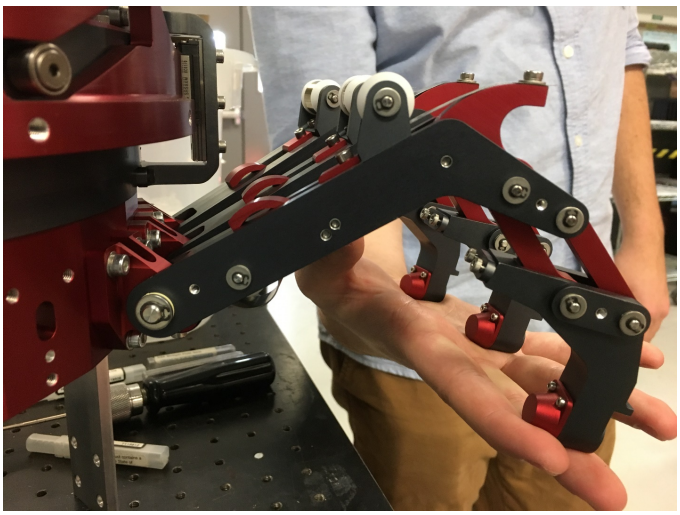

Figure 5: The final linkage design for ARM being installed on the tool body.

materials with small surface features such as rhyolite, the single large hook was unable to dig in and performed poorly while a large number of individual, small hooks were able to engage on the surface features and outperformed the single large hook. In both cases, there is not a significant difference in the performance of the arrays of the the small, medium, and large hooks. Based on these results, the cassette of smaller hooks was selected for the ARM gripper since it exceeded the 10% WOB requirement on all of the simulates.

The linkage used on the JPL-Nautilus gripper (shown diagrammatically in Fig. 7) is based on the final ARM gripper linkage and duplicates its basic kinematics. Unlike the ARM gripper linkage, the JPL-Nautilus gripper linkage uses a single megalodon hook since this simplifies the design and increases the grasp force when anchoring to softer materials. It also includes a different tendon routing and actuation scheme to enable object gasping in addition to anchoring. The 7/64" dyneema flexor tendon is routed from its termination on the distal link across an idler pulley (Harken 415 16 mm sheave) in the proximal

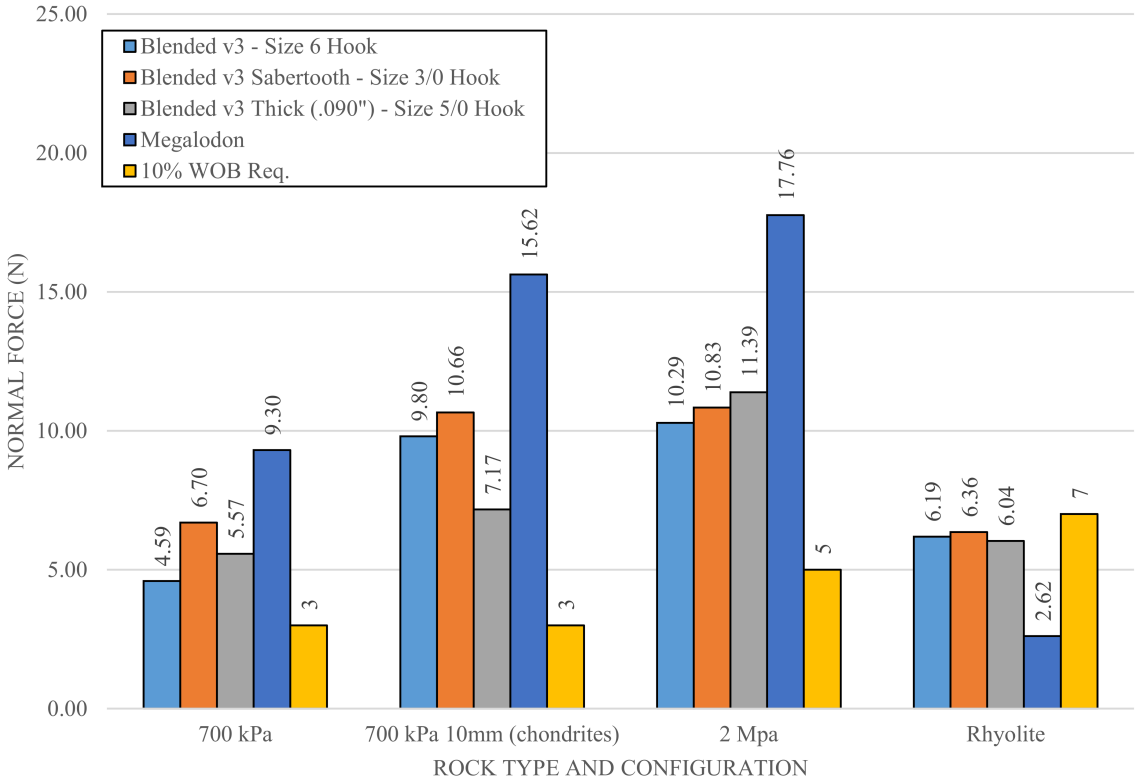

Figure 6: A comparison of the WOB (normal force) produced by a single linkage for cassettes of various hook sizes and for a single rigidly mounted megalodon hook when grasping a simulated 4 m diameter sphere. Performance of the megalodon hooks is consistently better than cassettes of smaller hooks for the soft comet simulant materials.

link and about a free spinning pulley (Harken 277 22 mm sheave) at the base of the digit, resulting in a moment about the base joint equal to the tendon tension times the pulley radius ($F_T \times r_p$) and a force applied to the distal joint equal to the tendon tension minus the force applied by the return spring ($F_T - F_{spring}$). These forces result in a normal force ($\frac{F_T \times r_p}{\ell}$) and shear force ($F_s = F_t - F_{spring}$) at the hook tip as shown in Fig. 7.

When actuated, the extensor tendon is released and the flexor tendon rotates the digit about the proximal joint until the spine is pressed against the grasp surface. Once all of the digits makes contact with the environment, the tendon tension rises until it is greater than the distal joint return spring's preload at which point the distal link is pulled inwards until the spine catches on a feature, fully constraining the digit. If the digit fails to make contact with the environment or catch on a feature, the linkage includes both proximal and distal joint travel limits and it will continue to close until both travel limits are reached.

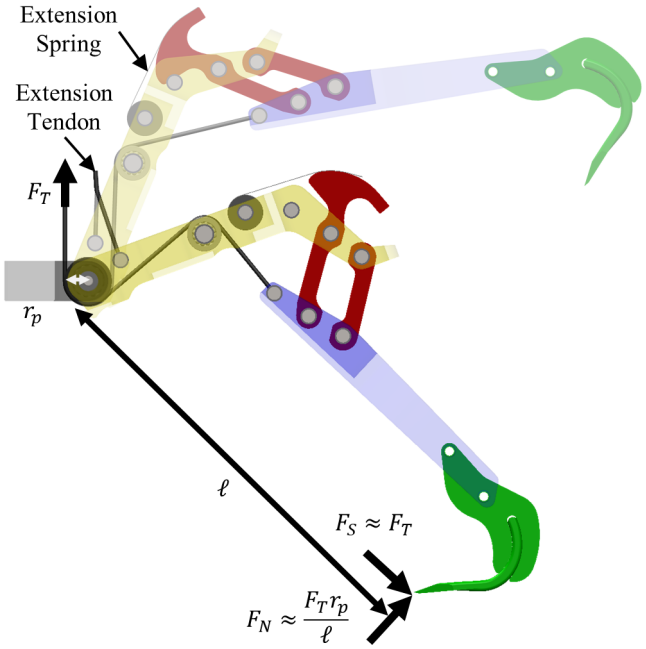

Figure 7: Diagram of the JPL-Nautilus gripper linkage in a open (transparent) and partially closed configuration. Each digit of the JPL-Nautilus gripper consists of a base (grey), proximal link (yellow), four-bar linkage (red), distal link (blue), and spine (green). The linkage is actuated by a flexor tendon that is routed across idler pulleys in the base and proximal link and terminates at the base of the distal link. The digit is opened by an extension tendon terminating on the proximal link and and an extension spring acting on the four bar linkage. The linkage dimensions were selected to provide 50 mm of translation of the spine while maintaining near constant spine angle with respect to a curved grasp surface.

2.2 Gripper Design

The gripper is composed of 16 identical digits radially arrayed about its center. The number of digits used in this prototype was chosen as a reasonable compromise between grasp strength and overall gripper size. All of the digits are actuated simultaneously with equal force through a 16 to 1 differential consisting of a continuous loop routed through 32 pulleys (Harken 404 16 mm Block) (see Fig. 8) [Jiang et al., 2015]. The input of the differential is a single plate that is mounted on and actuated by a lead screw and pair of linear bearings so that it can translate up and down. The input carries 16 pulleys while the outputs are the pulleys attached to each of the 16 flexor tendons. The output pulleys are connected to the input stage by the continuous tendon loop that snakes back and fourth between the two sets of pulleys. Since the length of the tendon loop is a fixed, translation of any of the output pulleys with respect to the input results in the remaining pulleys moving the opposite direction to keep the loop tendon taught. Similarly, ignoring friction, the tension in the loop must be constant so it must also apply equal force to all of the output pulleys regardless of their relative positions. This differential motion between fingers allows the gripper to adapt to large variations in the grasped surface geometry without sensing or active control since each digit can simply stop moving when it makes contact. After all 16 digits make contact and engage on features, the gripper is fully constrained and further increases

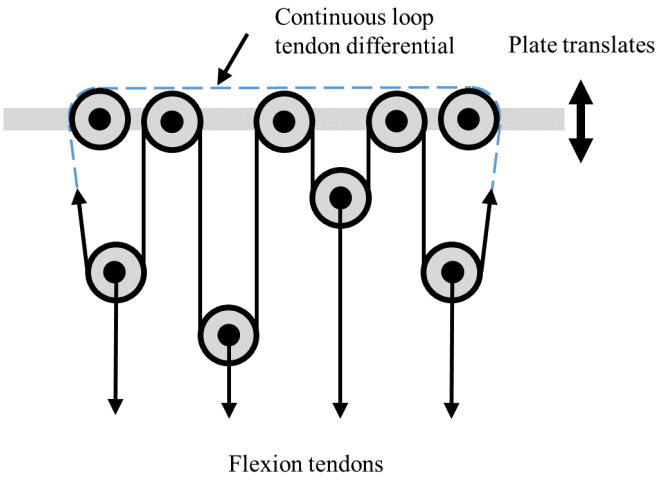

Figure 8: Equal force is applied to all of the digits via a continuous loop differential mechanism, shown here diagrammatically. The input to the differential is the translating plate and the outputs are the flexion tendons. Equal force is applied to the outputs by a single tendon that is routed through the pulleys, alternating between input and output pulleys and spliced to create a continuous loop.

in actuator force will cause the grasp force to increase proportionally. Because the input is driven by a position controlled actuator, compression springs (Century Spring Corp. AA-86) have been added in series with the pulleys mounted to the input plate to add compliance to the system and prevent sudden spikes in the force applied to the digits as the gripper is actuated.

To simplify integration with the ROV, the gripper is designed to be picked up by the parallel jaw end effector on the ROV's robotic arm via an industry standard 3/4" T-bar handle and is actuated via the redundant wrist rotation degree of freedom in the robotic arm as shown in Fig. 2. The T-bar handle is mounted to the body of the gripper via a slewing bearing (IGUS PRT-01-100-H1) and the body of the gripper is rotationally restrained by a bar braced in a collar mounted to the wrist of the robotic arm. Therefore, when the robotic arm's end effector is rotated, the body of the gripper remains stationary while the T-bar handle rotates. Rotation of the T-bar handle in turn is coupled to the lead screw (IGUS PTGSG-18x4-01-R-ES) that actuates the input to the differential. For laboratory testing, the T-bar handle was removed; instead, the gripper was directly mounted to the test stand and the lead screw was actuated via a electric motor with a 12 to 1 gear reduction (Maxon 347032). Based on the actuator and lead screw specifications and estimated frictional losses, we estimate that the actuator applied a flexor tendon tension to each digit of between 50 and 120 N when driven at 4 amps and 130 to 310 N when driven at 9 Amps.

3 Quantitative Gripper Evaluation

A series of tests were conducted in the laboratory to evaluate the JPL-Nautilus Gripper's object grasping and rock anchoring capabilities. First, its object grasping abilities were characterized by grasping a variety of different objects. Next, its capabilities as an anchor were assessed by grasping a repre-

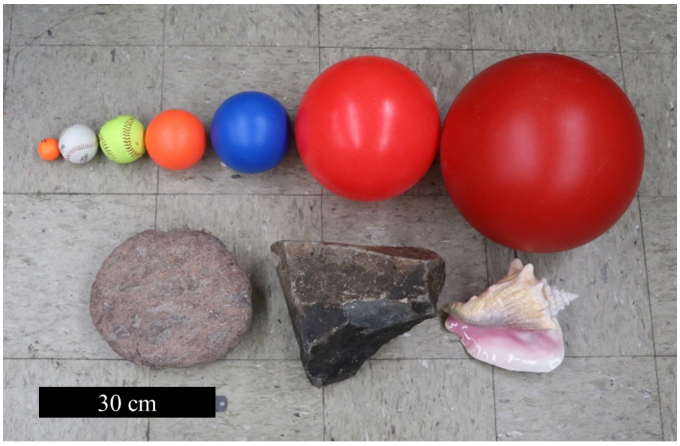

Figure 9: The gripper's object grasping performance was evaluated by grasping a range of test objects, shown here. These included 4.3, 7.4, 9.7, 11.4, 15.2, 25.1, and 33.5 cm diameter spheres, a small rock, a large rock, and a sea shell.

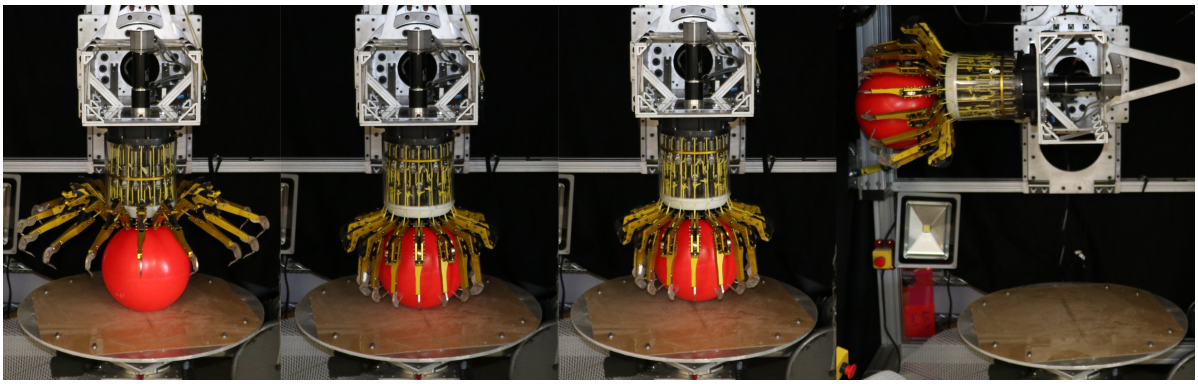

Figure 10: The object grasping performance for each object was evaluated by placing the object below the gripper, grasping it, lifting the gripper, and then rotating it as shown in this sequence of images (left to right). The quality of a grasp is scored based on if the object remains in the gripper when it is lifted and if it does not shift when the gripper is rotated.

sentative surface and measuring the normal and shear loads that the gripper could counteract under various conditions. The overall surface geometry, surface texture, and material strength were varied by conducting tests on multiple rock types in multiple orientations.

3.1 Object Grasping Methods

The gripper's object grasping performance was characterized by attempting to grasp a number of objects of different sizes and shapes under various conditions and scoring each trial based on the success or failure of the grasp using a procedure adapted from the YCB Gripper Assessment Protocol [Calli et al., 2015, YCB Benchmarks Main Page, 2016]. Although not representative of the irregular objects that may be found in the field, grasp testing focused primarily on spherical objects since their symmetry meant that the orientation of the object in the grasp would not have an effect on the result. The set of

test objects (shown in Fig. 9) consisted of seven spheres ranging in size from 4.3 to 33.5 cm in diameter, two different representative rocks, and a sea shell. A grasp trial is summarized in the sequence of images shown in Fig. 10. First, the gripper was opened and positioned 25 cm above a smooth acrylic sheet to allow the digits to swing through their full range of motion. If the object was more than 25 cm in diameter, the gripper was raised until the object fit between the palm and the sheet and the actual height above the sheet was recorded. Next, the object was positioned at the target point on the sheet, centered below the gripper. Then the gripper was closed by applying a constant current to the actuator to limit the closure force applied by the gripper. The motor current was selected empirically by the operator for each object. At least 4 amps was needed to overcome the internal friction within the gripper mechanism and was used when grasping the smaller, lighter objects. Higher closure force was needed to successfully grasp the larger, heavier objects and it was determined that driving the motor with 9 amps was sufficient for the large objects that were tested.

Once the motor stalled, the gripper was lifted until the object was at least 1 cm above the surface and the grasp was scored. The gripper was then rotated by 90° to test the security of the grasp and scored again. If the object remained in the grasp without any visual motion, the grasp was awarded two points, if it shifted but remained in the grasp, it was awarded one point, and if the object fell out of the grasp, zero points were awarded. This scoring approach was applied five seconds after grasping and lifting the object and again five seconds after rotating the gripper. Each test condition was repeated three times, and the scores from the trials for each test condition (grasp (G) and rotation (R)) are summed and converted to a percentage where 100% corresponds to a perfect score of six. To evaluate the gripper's tolerance to alignment error, the grasp trial for each object was repeated with the object offset horizontally (+10 cm X) and vertically (+5 and -1.5 cm Z) from the optimal target position and with the palm of the gripper rotated with respect to ground (palm angles of 18° and 30°). When the palm of the gripper was rotated with respect to the ground, the object was offset laterally to keep it within the gripper's workspace and the lateral offset was recorded. Lastly, the irregular objects were also grasped when placed on a bed of sand when centered below the gripper.

3.2 Object Grasping Results

Fig. 11 shows examples of the gripper grasping some of the test objects and Tables 1 and 2 summarize the results of the object grasping tests, including the object properties (mass and size), test parameters (motor current and palm height), and grasping results. The total score (expressed as a percentage) for each test case is reported after the object is picked up (G) and after the gripper is rotated (R). A dash symbol indicates the corresponding case was not tested because the gripper failed to grasp an easier case; for example the gripper failed to grasp a golf ball when centered below the gripper so it was not tested when offset in X or Z. For cases where the palm angle was not zero, the height of the gripper and the lateral offset of the object are reported for each trial.

As shown in Table 1, the gripper was capable of grasping a wide range of objects. When the objects were positioned at the center, the gripper successfully grasped spherical objects from 9.65cm to 33.5 cm in diameter, the lighter rock, and the sea shell in every trial. It also was able to grasp the baseball and

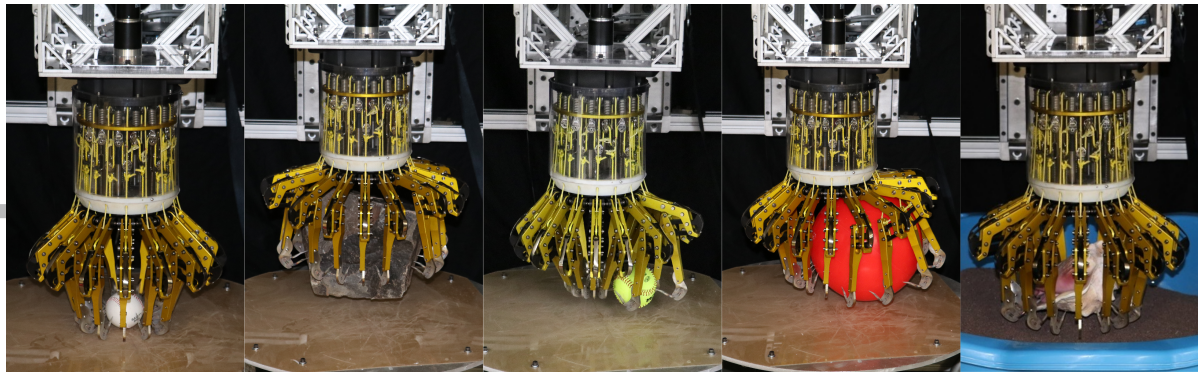

Figure 11: The JPL-Nautilus Gripper is capable of grasping a range of different objects, examples of which are shown here. The baseball and large rock were grasped from the target position, the softball and XL ball were displaced laterally, and the seashell was grasped from a bed of sand. The grasp of the baseball failed while the grasps of the softball, XL ball, rock, and seashell were successful.

Table 1: Object Grasping With Position Error Test Result

	Object	Mass (g)	Diam. (cm)	Current (A)	Palm Height	Centered G	Centered R	+10 cm X G	+10 cm X R	+5 cm Z G	+5 cm Z R	-1.5 cm Z G	-1.5 cm Z R	Palm Height	Sandy G	Sandy R
Spherical Objects	Golf ball	46	4.3	4	25 cm	0	0	-	-	-	-	-	-	-	-	-
	Baseball	140	7.4	4	25 cm	33	33	33	33	-	-	100	33	-	-	-
	Softball	170	9.7	4	25 cm	100	100	100	100	0	0	100	100	-	-	-
	S ball	139	11.4	4	25 cm	100	100	100	100	0	0	100	100	-	-	-
	M ball	251	15.2	4	25 cm	100	100	100	100	0	0	0	0	-	-	-
	L ball	803	25.1	9	25.3 cm	100	100	100	100	100	100	-	-	-	-	-
	XL ball	1,030	33.5	9	33.6 cm	100	100	100	100	100	0	-	-	-	-	-
Other Objects	S rock	9,290	27x23x10	9	25.3 cm	100	100	100	0	-	-	-	-	25.2 cm	100	50
	L rock	20,600	25x30x25	9	25.3 cm	50	16.7	50	0	-	-	-	-	25.2 cm	50	50
	Seashell	1,310	24x22x11	9	25 cm	100	100	66.6	33.3	16.7	0	100	50	25.3 cm	100	50

larger rock (shown in Fig. 11) some of the time. When grasping the golf ball and baseball, the geometry of the spines resulted in the tips of the spines contacting the smaller objects above the objects' widest point, resulting in a grasp attempt that did not cage the object. Since the objects lacked features for the spines to catch on, the spines tended to then slide across the upper surface and eject the object, causing the grasp to fail. Similarly, due to the shape of the large rock (show in Fig. 11), the digits were unable to scoop under the rock and instead engaged on its flat vertical sides. Since the particular rock was relatively smooth, the spines only caught on asperities some of the time, resulting in inconsistent results. The gripper's ability to grasp smaller objects or objects with less undercut sides such as the large rock may be improved by redesigning the geometry of the spine holder (shown in green in Fig. 7) to reduce the distance that it projects past the tip of the spine. Doing so will allow the tip of the spine to be closer to the ground when the spine holder makes contact and will allow the spine to scoop under and cage smaller objects.

The gripper's performance is also reasonably robust to lateral position errors (+10 cm X). Under these conditions, its performance when grasping the spherical objects is unchanged while it exhibits moderately lower success when grasping the rocks and seashell. However the resulting grasps look significantly different when the object is translated 10 cm horizontally relative to the gripper. Instead

Table 2: Object Grasping With Palmer Misalignment Test Result

	Object	Mass (g)	Diam. (cm)	Current (A)	Palm Height	Palm Angle 18° offset	Palm Angle 18° G	Palm Angle 30° offset	Palm Angle 30° G
Spherical Objects	Golf ball	46	4.3	4	-	-	-	-	-
	Baseball	140	7.4	4	22 cm	12 cm	0	19 cm	-
	Softball	170	9.7	4	22 cm	12 cm	100	19 cm	0
	S ball	139	11.4	4	22 cm	12 cm	100	19 cm	0
	M ball	251	15.2	4	22 cm	12 cm	100	19 cm	100
	L ball	803	25.1	9	26.7 cm	12 cm	100	9 cm	100
	XL ball	1,030	33.5	9	36 cm	7 cm	100	4 cm	0
Other Objects	S rock	9,290	27x23x10	9	22 cm	12 cm	100	7 cm	16.7
	L rock	20,600	25x30x25	9	24.5cm	7 cm	83.3	6 cm	0
	Seashell	1,310	24x22x11	9	22 cm	2 cm	100	7 cm	100

of pulling the object into the center of the gripper, the digits conform to the object at its offset position as can be seen in the examples of grasps of the softball and XL ball shown in Fig. 11.

However, the gripper's object grasping performance is very sensitive to the vertical position error. Moving the gripper up 5 cm results in it failing to grasp all but the two largest spheres and seashell since the spines no longer scoop under the smaller objects. Moving the gripper down 1.5 cm results in more success when grasping the baseball since the spines engage lower on its surface but prevents the gripper from grasping larger objects that no longer fit between the grippers palm and the ground. Lastly, further lowering of the gripper causes grasps to fail since the closing trajectory of the digits passes through the ground and therefore the gripper is unable to close fully.

The gripper was also tested grasping the natural objects (rocks and seashells) when placed on a sandy substrate and the results of these tests are summarized in the rightmost section of Table 1 under the heading Sandy. Under these conditions, the hooks can trench through the sand and potentially scoop further under the objects. Although we would expect this to improve the gripper's performance, we observed similar grasp performance in comparison to the original test case. Furthermore, the grasps of the small rock and seashell were less robust while the grasp of the large rock was more robust than when these objects were grasped off of a smooth surface.

Testing, summarized in Table 2, also showed that the gripper is robust to moderate palmer misalignment with the ground if the palm height and lateral offset are adjusted appropriately. Grasp performance is not significantly degraded when the palm is misaligned by 18° but performance does degrade when when the palm is misaligned by 30°. Intuitively this makes sense: when grasping a spherical object, the direction the gripper approaches from should not matter since the object is radially symmetric. However, if a change in the approach direction causes the digits to contact the environment before the object, this environmental contact may alter the resulting grasp and cause it to fail. In these test cases, rotating the gripper by 18° with respect to the ground did not substantially alter when the digits contacted the ground relative to the object but did change the position of the object with respect to the gripper's coordinate frame. Offsetting the object and adjusting the height of the gripper compensates

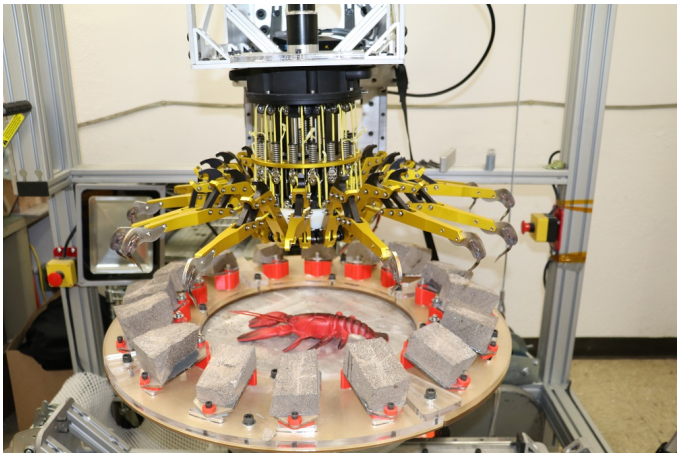

Figure 12: The anchoring capabilities of the gripper were evaluated by measuring the force the gripper could counteract when attached to various substrates using the test setup shown here. Individual rock coupons were mounted to a large plate that is in turn mounted to a six axis load cell (not shown). The coupons and plate act like a single large rock and the load cell measures the net forces applied to the simulated rock by the gripper.

for the change in relative position and under these conditions the gripper grasped all but the golf ball, baseball, and large rock successfully in all trials. In contrast, when rotated 30° with respect to the ground, some of the digits collided with the ground before they could scoop under the object, and as a result the gripper was only able to grasp the medium and large balls and seashell reliably.

3.3 Asperity Grasping Methods

The gripper's asperity grasping abilities (its ability to anchor to rough textured surfaces) were characterized by engaging the gripper on a number of different rock types and gross surface geometries and measuring the normal and shear loads that the grasp could counteract in each case. To simulate anchoring to a large rock, individual rock coupons (approximately 6 by 9 cm) were positioned below each of the digits and mounted to a six axis load cell (ATI-OMEGA160) as shown in Fig. 12. At the start of a trial, the load cell was tared and the applied loads were then recorded throughout the remainder of the trial. Next, the gripper was lowered until the palm would contact the surface of the simulated rock (assumed to be the sphere tangent to the surfaces of the rock coupons). Then, the gripper was actuated with constant current until the motor stalled. The current was limited to 3 amps (applying an estimated flexor tendon tension between 40 to 97.6 N) for the dry testing and 2 amps (applying an estimated flexor tendon tension between 25 to 62N) for the submerged testing since this was sufficient to overcome the internal mechanism friction but not high enough to cause the weaker rocks to fail. The motor position was then locked and the grasp strength was measured by loading the grasp in the normal (z) or shear (x) direction until the grasp failed or the measured force exceeded 450 N. Each of the normal loading conditions trials was repeated five times and each of the shear loading cases was repeated three times. The maximum normal or shear force observed in each trial is then recorded and the mean and standard deviation are reported here.

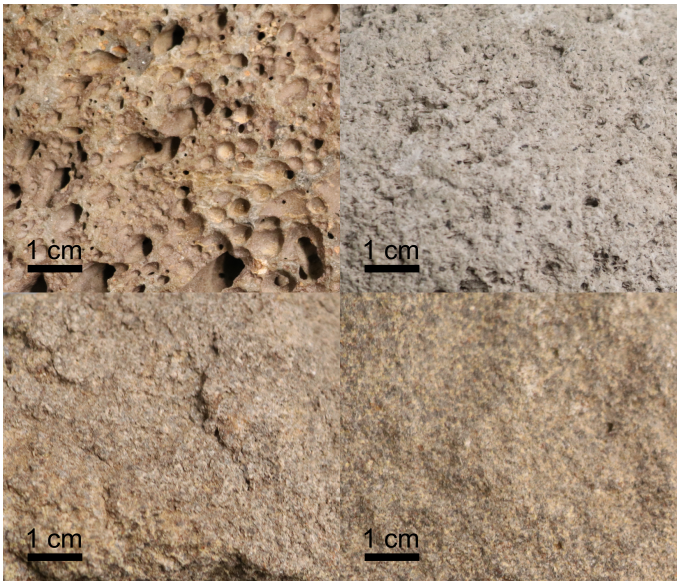

Figure 13: The asperity grasping performance of the gripper was evaluated on various different rock types. Images of the surfaces of the rock suite including vesicular basalt (a), pumice (b), heavily-weathered basalt (c), and lightly-weathered basalt (d) are shown here.

The impact of the convexity of the rock was investigated by varying the angle of the individual coupons to simulate both flat surfaces (0°) and rocks with a radius of curvature of approximately 2 m (15°). The sensitivity of the gripper to angular misalignment was also investigated by repeating the test conditions with the lightly-weathered basalt when the palm of the gripper was rotated 5 and 10 degrees from horizontal. The type of rock used on the coupon was also varied to investigate the impact of both surface texture and rock strength on the grasp. Tests were conducted with vesicular basalt, pumice, heavily-weathered basalt, and lightly-weathered basalt rock samples, examples of which are shown in Fig. 13. These rocks were selected based on their resemblance to samples of various rocky surfaces found on the seafloor including dense and scoriaceous lava, manganese crusts, and carbonate crusts. The vesicular basalt represented the most featured and strongest rock that was tested. The pumice was also highly featured but the features were smaller than those found on the vesicular basalt and the overall rock was weaker. Both the more and lightly-weathered basalts had grain like surface features that could fail easily in comparison to the vesicular basalt and pumice. However, features on the heavily-weathered (altered) basalt tended to be larger and weaker in comparison to those on the lightly-weathered basalt.

3.4 Asperity Grasping Results

Table 3 summarizes the results of the asperity grasp testing. For each test, we report the the mean and standard deviation of the normal and shear loads that the grasp was able to counteract in air and the normal load when submerged in water. The results show that, the surface texture and strength of the rock had the largest impact on the gripper's performance: grasps of stronger, more featured rocks tend to counteract higher loads. Surface curvature, expressed in terms of coupon angle, also effected the grasp

Table 3: Asperity Grasping results

Rock Type	Coupon Angle	Palm Height	Palm Angle	Loading Condition				Submerged Testing	
				Normal		Shear		Normal	
				mean	σ	mean	σ	mean	σ
Vesicular Basalt	0°	0 cm	0°	236 N	127 N	498 N	46.0 N	236 N	86.2 N
	15°	5.8 cm	0°	465 N	68.8	465	11.6	457	50.1
Pumice	0°	0 cm	0°	32.5 N	17.4	180	20.5	17.4	2.74
	15°	5.8 cm	0°	102 N	37.3	193	20.5	20.9	10.2
Lightly-weathered Basalt	0°	0 cm	0°	0	-	172	93.0	1.79	4.07
	0°	0 cm	5°	0	-	235	40.8	-	-
	0°	0 cm	10°	0	-	197	31.3	-	-
	15°	5.8 cm	0°	12.8 N	10.8	154	31.8	2.44	7.76
	15°	5.8 cm	5°	12.0 N	7.92	140	6.24	-	-
	15°	5.8 cm	10°	12.5 N	9.04	121	39.7	-	-
Heavily-weathered Basalt	0°	0 cm	0°	12.6 N	4.54	187	19.1	16.3	7.75
	15°	5.8 cm	0°	62.4 N	33.4	109	39.0	48.3	28.9

strength. In all cases, increasing the coupon angle increased the normal force that the grasp could resist. However, the coupon angle had little effect on the shear force the gripper could oppose. Surprisingly, moderate palmer misalignment (measured in terms of the angle between the object's surface and the gripper's palm) and grasping underwater do not appear to impact the shear and normal loads that the gripper can support.

Rock type has a significant impact on the grippers performance resisting normal and shear loads. It performed best when grasping the vesicular basalt, a highly featured and strong rock. When grasping this type of rock, the spines were able to engage in the vesicles and provided a very secure grasp capable of counteracting 236N on average when anchored to a flat rock. When anchored to the angled coupons, the grasp strength increased and most tests were terminated when the applied load exceed 450 N. Similarly, the shear load tests for both flat and angled coupons were also terminated when the 450 N force threshold was exceeded. The next strongest grasps were observed when grasping pumice, a weaker rock with smaller pores. In this case, the spines were also able to engage in the pores resulting in secure grasps. However due to the smaller features and weaker rock, the rock would often fail or the hook would slip off of a feature when sufficient load was applied, limiting the average force that a grasp could support to 32.5 N on flat coupons, 102 N on the angled coupons, and approximately 186 N in shear. Grasps of the heavily-weathered basalt were able to support the third highest normal loads. This rock is nonporous and has a rough textured surface that the hooks were able to engage on. However the surface features and bulk rock itself are quite weak and would often crumble when loaded, causing a grasp to fail at relatively low loads (12.6 N on flat coupons, 62.4 N for the angled coupons, and between 109 N and 187 N in shear). Lastly, the lightly-weathered basalt resulted in the weakest grasps (0 N for the flat coupons, 12.8 N for the angled coupons, and 163 N in shear on average). When grasping the flat coupons, the gripper failed to grasp entirely and simply pushed itself away from the substrate. Although the lightly-weathered basalt is stronger than the heavily-weathered basalt, it has finer surface features that the spines could not always engage on, potentially explaining the extremely poor grasping performance that we observed.

Coupon angled (θ) also had a large effect on the normal loads the gripper could counteract. For each rock type, the gripper performed substantially better when grasping the angled coupons (equivalent to a rock with a radius of curvature of approximately 2 m). This performance improvement makes intuitive sense: if we assume that each spine can exert a given normal (F_n) and shear (F_s) force on an asperity before failing, the total normal force that the gripper can resist may be estimated by summing the components of the individual contact forces that are in the gripper normal direction. Since the gripper is radially symmetric, the contribution from each digit may be expressed as follows: $F'_n(\theta) = F_n \cos(\theta) + F_s \sin(\theta)$ where F_s is tangent to and F_n is normal to the surface at the contact point and F'_n is perpendicular to the palm of the gripper. When the coupons are flat ($\theta = 0°$), only the contact normal forces (F_n) resist the normal force applied to the gripper. However, when the coupons are angled ($\theta = 15°$), the contribution from the normal force is only reduced slightly while the contribution from the shear force is substantial ($F'_n(15°) \approx 0.97F_n + 0.26F_s$). Furthermore, prior work has shown that the adhesion limit ($\alpha = \arctan(F_n/F_s)$) varies significantly with material [Asbeck and Cutkosky, 2012]. For materials with small adhesion limits, the shear component of the contact force is large in comparison to the normal component, further improving the apparent performance of the gripper on curved surfaces. In contrast, altering the coupon angle has no detectable effect on the shear forces that the gripper can support for the vesicular basalt, pumice, and lightly-weathered basalt and increasing the coupon angle results in a reduction of the shear load for the heavily-weathered basalt.

Lastly, operating the gripper under water has little to no effect on its performance. Its performance was unchanged when grasping the vesicular basalt, flat pumice, 15° lightly-weathered basalt, and heavily-weathered basalt when submerged in fresh water. However, it performed worse when grasping the 15° pumice and better when grasping the flat lightly-weathered basalt based on a 95% confidence interval two sample t-test comparison of the results. One possible explanation for this is that the water weakened these rock samples, causing the pumice to fail more easily and resist lower loads. Although we expect that the lightly-weathered basalt would also have been weakened by the water, in this case it may have allowed the spines to dig into the rock more. The increase in grasp strength from greater engagement of the spines into the rock may then have more than offset the loss of strength of the rock. However further testing is needed to investigate these conjectures and determine the explanation for these observations.

4 Field Testing

In order to further validate the gripper's design, its suitability for use in the field, and interoperability with ROVs, it was tested aboard the E/V Nautilus on cruise NA101 in the Papahānaumokuākea Marine National Monument. During this field trial, we tested the gripper's object grasping performance by picking up loose rocks from the sea floor and its asperity grasping capabilities by grasping large boulders and rock faces when teleoperated with the ROV Hercules at depths over 2000 meters on dives N1715, N1720, and N1723. Prior to conducting these dives, integration and operation of the gripper by the ROV was confirmed via deck testing: the gripper and cradle were positioned on the front of the ROV and oriented so that the Kraft Predator robotic arm, a hydraulically actuated six degree of freedom arm capable of lifting 200 lb at full (79 in) extension [TeleRobotics, 2005], could grasp the T-bar handle and

Figure 14: Before deploying the gripper, its integration with and operation by the ROV Hercules was tested on deck. These images show the position of the gripper on the ROV when not in use (left) and how the gripper is picked (center) up and held by the robotic arm (right).

slide the brace bar into the slot in the wrist collar. The positioning and operational sequence was then validated by removing the bungee cord that secured the gripper, picking the gripper up, operating it through its full range of motion, and replacing it in the cradle via teleoperation from the ROV control van as shown in the sequence of images in Fig. 14. Successful deck testing and subsequent field operation confirmed that our integration approach that relied on storing the gripper in a cradle on the front of the vehicle and using the robotic arm to grasp and rotate a T-bar handle to operate the gripper was viable. Testing also showed that due to the limited mobility of the six degree of freedom arm, proper positioning of the gripper's cradle with respect to the arm was needed to allow the gripper to be picked up. Operations also showed the value of mounting the gripper's cradle on wire rope isolation mounts that allowed the cradle to translate up to 2 cm relative to the ROV. This compliance accommodated position and alignment errors of the gripper with respect to the cradle when it was picked up or returned.

4.1 Object Grasping in the field

Based on the successful integration testing, the gripper was deployed aboard the ROV on a number of dives to demonstrate its grasping and anchoring capabilities. When conducting an object grasp trial (an example trial is shown in Fig. 15), first the target object was identified in the ROV's video feed. Then the ROV pilot positioned the vehicle next to the object and positioned the gripper above the target object using the robotic arm. Once in position, the pilot closed the gripper by continuously rotating the robotic arm's wrist. Since this actuator did not provide fine force feedback, we were unable to replicate the motor current based force control used in the lab testing and instead halted the actuator based on the observed pose of the gripper. After concluding that the gripper had grasped the object based on visual observation, the robustness of an object grasp was tested by picking the object up and rotating the gripper with the robotic arm while observing if the grasped object shifted relative to the gripper.

Examples of the objects of opportunity that we grasped on the sea-floor are shown in Fig. 16. These

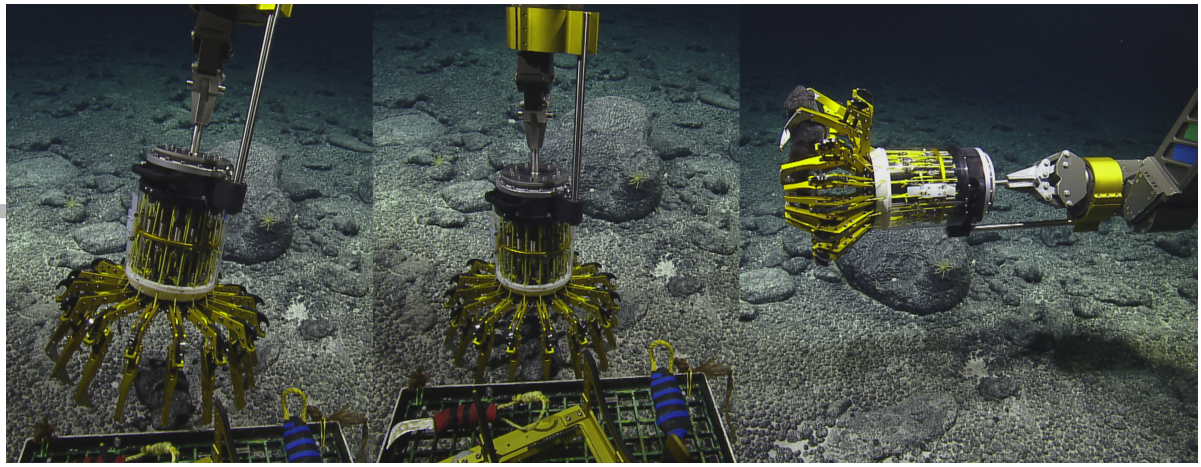

Figure 15: The object grasping test was repeated in the field with the ROV Hercules at approximately 2000m depth. This sequence of images shows a representative object grasping field trial where the gripper was positioned above the target rock found in situ on the seafloor (left), closed to grasp the rock (middle), and picked up and reoriented to test the grasp robustness (right). Copyright Ocean Exploration Trust, Inc.

trials show that the gripper can be used to pick moderately sized (10 - 30 cm), irregular rocks similar to those tested in the lab from relatively smooth surfaces. Although these objects were successfully grasped, testing revealing a number of limitations of the current system. First, the lack of force control or feedback made it difficult for the operators to correctly judge when the gripper had closed fully. Since the operators did not wish to damage the gripper by over-tightening it, insufficient grasp force was often applied, resulting in failed initial grasps. Secondly, the length of the gripper from the top of the T-bar handle to the palm of the gripper (approximately 47 cm) when combined with the workspace limitations of the robotic arm meant that it was difficult to properly position the gripper above objects near the front of the ROV. The length of the gripper also prevented us from depositing any of the grasped objects in the vehicle's sample bins since the gripper could not be positioned above them. Lastly, the closing trajectory of the digits and geometry of the spine made it difficult to grasp objects positioned in a depression or surrounded by other objects.

4.2 Asperity Grasping in the field

Asperity grasps trials were conducted in a similar fashion: after identifying a grasp target, the ROV was positioned near the target by the pilot and either landed on the sea floor or placed into a position holding mode. Next, the gripper was opened fully and the palm was pressed against the grasp target using the robotic arm. Then, the gripper was closed by rotating the arm's wrist. The state of the grasp was estimated based on observing if individual digits continued to reconfigure as the wrist was rotated and when possible, by observing the degree to which the springs in the differential had compressed. After determining that the gripper had engaged on the grasp target, the strength of the grasp was evaluated. In the initial tests, the security of the grasp was tested by pulling up on the gripper with the robotic arm, yielding a binary result - either the gripper was pulled off or not. In later tests, the

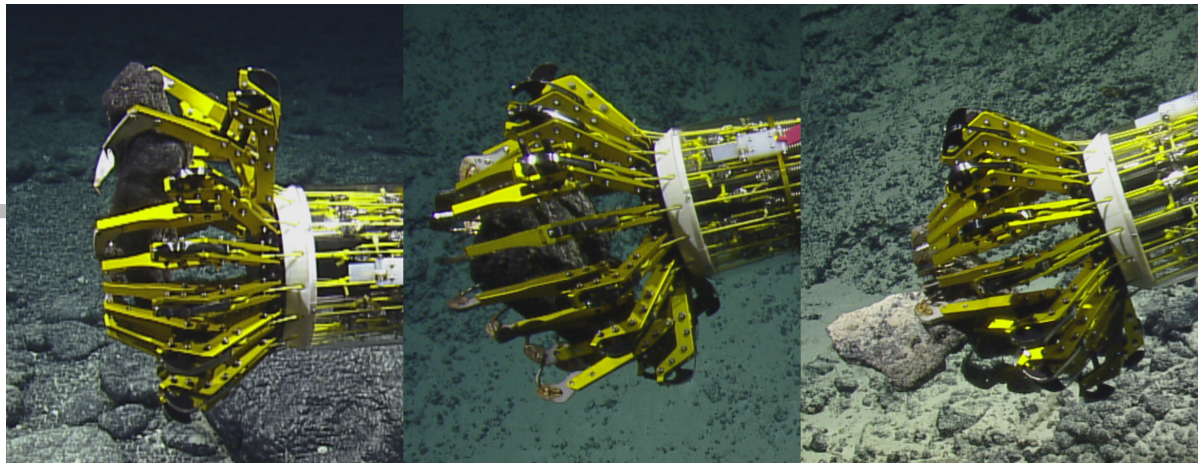

Figure 16: The JPL-Nautilus gripper was able to grasp different size and shape objects from the seafloor when operated by the ROV Hercules at approximately 2000m depth, examples of which are shown here. Copyright Ocean Exploration Trust, Inc.

ROV's thrusters were used to apply various loads to the gripper and the applied thrust was estimated and recorded based on the percent the thruster hydraulic valves were opened. First, the gripper was loaded normal to the palm - either backing away from a vertical face or thrusting upward if anchored to the sea floor. Then if the gripper remained attached, a moment was applied by commanding a vehicle heading change. In both cases, the thrust was gradually increased until it exceeded approximately 30 lbs ($\approx$ 20% of the ROV's maximum) and the grasp was considered secure if it did not fail under this load.

Examples of various asperity grasps are shown in Fig. 17. These tests demonstrated that the gripper is capable of robustly securing itself and the ROV to a variety of surfaces found on the seafloor including boulders, lava pillows, and rock faces. In these trials, the strength of the grasp varied significantly from trial to trial based on the strength of the underlying rock, the surface texture, gross curvature of the surface, the position of the individual spines on the surface, and the loading direction. The gripper performed best when grasping weak rocks that the spines could dig into (Fig. 17 bottom left), curved surfaces that the digits could wrap around (Fig. 17 top left), and irregular surfaces with larger, more positive features for the spines to engage on (Fig. 17 top and bottom center). In these cases, the resulting grasps were secure even when disturbances, including normal and bending moment loads of approximately 100 N were applied via the vehicle's thrusters.

In the example shown in the bottom right image of Fig. 17, a strong current perpendicular to the vehicle caused the vehicle to rotate about the gripper applying a torsional load to the grasp and eventually causing the grasp to fail. This loading case exerts a large moment on the gripper due to the large moment arm that the ROV presents and has not been considered in the design or testing of the gripper to date. However, intuitively this loading case should result in a lateral load at each spine that would cause the spines to slide sideways off of the asperities they are engaged on and therefore may represent a unforeseen grasp failure mode. However, the gripper is unlikely to be loaded in this fashion when

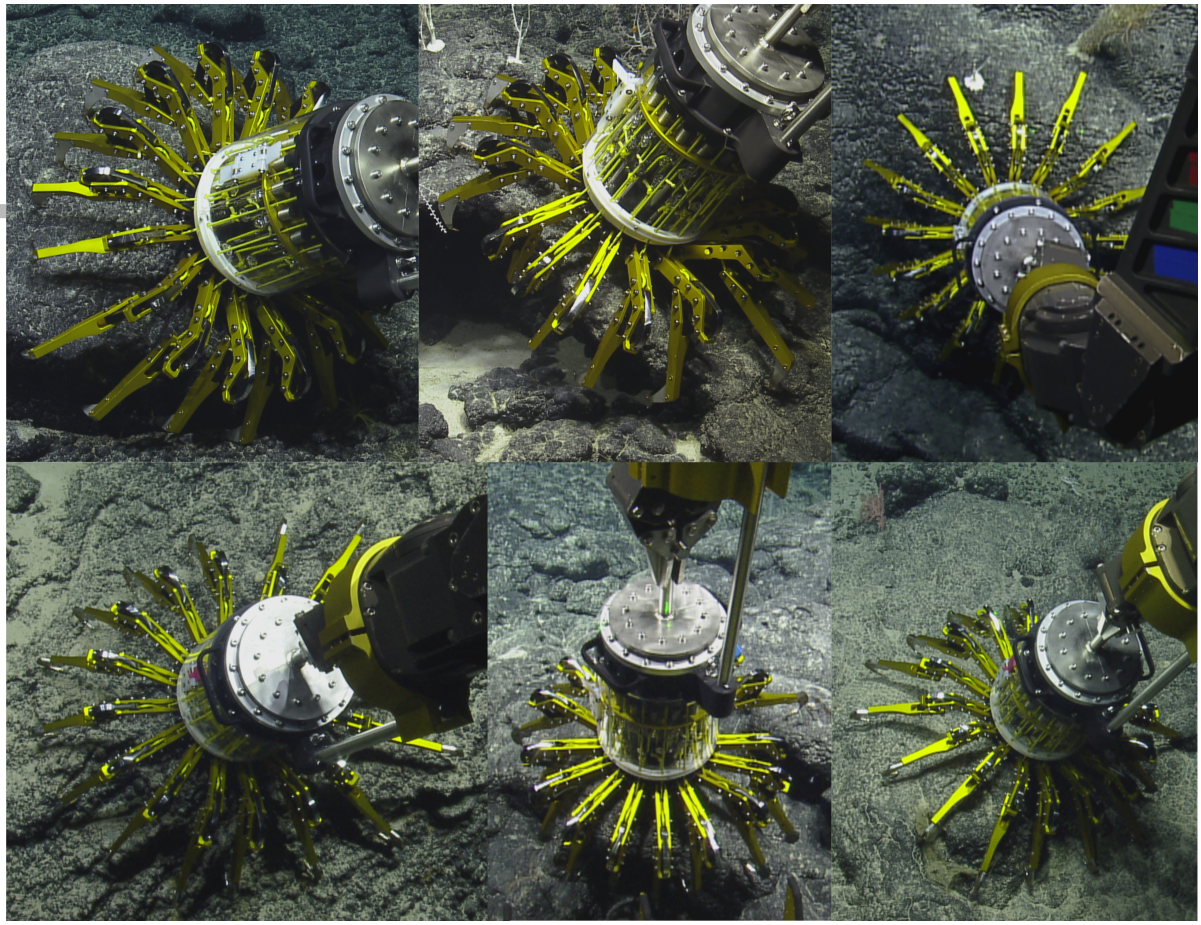

Figure 17: During the field test, the JPL-Nautilus gripper successfully anchored the ROV Hercules to a number of different exposed rocky surfaces found on seamounts in the Papahānaumokuākea Marine National Monument and images of some of these trials are shown here. Grasps on a boulder (top left), friable cliff face (bottom left), and irregular sea floor (bottom center) resisted all disturbances applied to them. When sufficient force was applied to the overhanging lip of rock (top center) by the gripper, the rock failed, breaking into multiple pieces, and the gripper detached. Lastly, when grasping the relatively flat manganese encrusted surfaces shown in the two rightmost images, the gripper resisted low loads but the grasp failed as the applied forces increased. Copyright Ocean Exploration Trust, Inc.

grasping vertical faces in front of the vehicle or when the position holding routines are engaged.

Grasps of flatter and smoother surfaces proved to be much weaker or fail entirely. For example, the grasp show in the top right images of Fig. 17 failed immediately once the vehicle's position holding routine was disabled. Other grasps of similar surfaces failed entirely or were very sensitive to the positioning of the gripper on the surface. In particular, when attempting to grasp a relatively flat surface, depressions and other surface irregularities altered the hook's contact angle and in some cases caused the tip of the hook to not contact the surface at all, increasing the chance that the grasp would fail. Based on this observation, increasing the angle of the hook with respect to the surface (currently 45°) and reducing the distance that the digit projects past the hook tip may help eliminate the cases where the hook tip fails to contact the surface.

5 Future Work

Based upon the successful laboratory and field test campaigns, we believe that we have demonstrated the viability of a microspine based anchor for stabilizing a rock sampling drill that is capable of anchoring to various rocky sea floor substrates. The next iteration of this gripper should include a coring drill capable of taking useful scientific samples located in the center of the existing microspine based gripper. The combined system will rely on the gripper to counteract the drilling loads and hold the free floating ROV in position while collecting rock samples from large rock formations in the deep ocean.

In addition to developing the integrated sampling tool, additional experimentation with the gripper may improve its object grasping and anchoring performance. Specifically, experimenting with both the spine contact angle and geometry of the tip of the digit may allow the digits to scoop under smaller objects, improving the grippers object grasping performance. It may also improve the anchoring performance in some scenarios where the current finger tip design collides with the environment, preventing the spine from engaging on the surface.

6 Conclusions

This paper summarizes the design, laboratory testing, and initial field trial of the JPL-Nautilus Gripper prototype, a marine microspine based gripper designed for use by a ROV. Secure grasping of spherical objects from 10 to 30 cm in diameter, rocks, and a seashell under moderate positional uncertainty was demonstrated in the the lab and this capability was further validated through grasping a number of rocks from a free floating ROV in the field. Anchoring to various rock types was also demonstrated. In the lab, asperity grasps on highly featured strong rocks resisted forces over 500 N and secure grasps were also achieved on weaker and less feature rocks. Similar performance was observed in the field: grasps on convex, featured surfaces resisted estimated applied loads over 100 N and did not fail while grasps on less featured surfaces failed at lower loads. These test results show that the gripper can be used to pick up rock samples and anchor the vehicle or other payloads to the sea floor in its current form. The test results also suggest that an improved version of the gripper may be capable of stabilizing a coring drill and exerting the necessary weight on bit ($\approx$ 100 N based on past experience [Parness et al., 2017a, Stakes et al., 1997]) required to collect rock cores from various substrates.

Acknowledgment

The research was carried out at the Jet Propulsion Laboratory, California Institute of Technology, under a contract with the National Aeronautics and Space Administration. Copyright 2020 California Institute of Technology. Government sponsorship acknowledged.

Field testing was conducted in cooperation with the Ocean Exploration Trust's *Nautilus* Exploration Program. The NA101 expedition was funded by the Ocean Exploration Trust and the NOAA Office for

Exploration and Research (grant NA17OAR0110336)). We would also like to thank the captain and the crew of the E/V Nautilus and the ROV Hercules team for making the field tests of the gripper a success.

Representative samples of seafloor rocks that were used to identify the suite of rocks used for laboratory testing were also provided by the URI/GSO Marine Geological Samples Laboratory and the National Science Foundation (grant OCE-1555523)

A Index to Multimedia Extensions

Extension	Media Type	Description
1	Video	This video shows examples of the gripper in use during the field test including how it was deployed and stowed and examples of successful object and asperity grasps.

References

Asbeck, A. T. and Cutkosky, M. R. (2012). Designing Compliant Spine Mechanisms for Climbing. *Journal of Mechanisms and Robotics*, 4(3). 031007.

Asbeck, A. T., Kim, S., Cutkosky, M. R., Provancher, W. R., and Lanzetta, M. (2006). Scaling hard vertical surfaces with compliant microspine arrays. *The International Journal of Robotics Research*, 25(12):1165–1179.

Backes, P., Moreland, S., Rehnmark, F., Badescu, M., Zacny, K., Wei, R., Adams, G., Toda, R., Vieira, P., Carey, E., Krylo, R., Martin, M. S., Bailey, E., Seubert, C., Conway, D., Aaron, S., Manohara, H., Peters, G., Mongelli, M., and Riccobono, D. (2017). Biblade sampling tool validation for comet surface environments. In *2017 IEEE Aerospace Conference*, pages 1–20.

Bemfica, J. R., Melchiorri, C., Moriello, L., Palli, G., and Scarcia, U. (2014). A three-fingered cable-driven gripper for underwater applications. In *2014 IEEE International Conference on Robotics and Automation (ICRA)*, pages 2469–2474.

Birglen, L., Laliberté, T., and Gosselin, C. M. (2007). *Underactuated robotic hands*, volume 40. Springer.

Calli, B., Walsman, A., Singh, A., Srinivasa, S., Abbeel, P., and Dollar, A. M. (2015). Benchmarking in manipulation research: Using the yale-cmu-berkeley object and model set. *IEEE Robotics Automation Magazine*, 22(3):36–52.

Carpenter, K., Wiltsie, N., and Parness, A. (2016). Rotary microspine rough surface mobility. *IEEE/ASME Transactions on Mechatronics*, 21(5):2378–2390.

Emerson, D. and Shank, T. (2016). Ecology and molecular biology. In *Developing Submergence Science for the Next Decade*, pages 48–52.

Deep Submergence Science Committee. Retrieved November 16, 2018, https://www.unols.org/sites/default/files/DESCEND2%202016%20FINALFINAL_small.pdf.

Galloway, K. C., Becker, K. P., Phillips, B., Kirby, J., Licht, S., Tchernov, D., Wood, R. J., and Gruber, D. F. (2016). Soft robotic grippers for biological sampling on deep reefs. *Soft Robotics*, 3(1):23–33. PMID: 27625917.

German, C. and Tominaga, M. (2016). Polar systems. In *Developing Submergence Science for the Next Decade*, pages 31–40. Deep Submergence Science Committee. Retrieved November 16, 2018, https://www.unols.org/sites/default/files/DESCEND2%202016%20FINALFINAL_small.pdf.

Greenberg, R., Stone, W. C., Kantor, G., Wettergreen, D., and Durda, D. D. (2005). The DEPTHX Project: Pioneering Technologies for Exploration of Extraterrestrial Aqueous Channels. In *56th International Astronautical Congress of the International Astronautical Federation, the International Academy of Astronautics, and the International Institute of Space Law*, pages 1–11, Reston, Virigina. American Institute of Aeronautics and Astronautics.

Hayman, N. and Perfit, M. (2016). Geology. In *Developing Submergence Science for the Next Decade*, pages 53–58. Deep Submergence Science Committee. Retrieved November 16, 2018, https://www.unols.org/sites/default/files/DESCEND2%202016%20FINALFINAL_small.pdf.

Jiang, H., Hawkes, E. W., Arutyunov, V., Tims, J., Fuller, C., King, J. P., Seubert, C., Chang, H. L., Parness, A., and Cutkosky, M. R. (2015). Scaling controllable adhesives to grapple floating objects in space. In *2015 IEEE International Conference on Robotics and Automation (ICRA)*, pages 2828–2835.

Josso, P. (2016). MarineE-tech research expedition blog JC142 cruise blog #3 geological sampling. Retrieved November 16, 2018, from http://marinee-tech.blogspot.com/2016/11/jc142-cruise-blog-3-geological-sampling.html.

Lane, D. M., Davies, J. B. C., Robinson, G., O'Brien, D. J., Sneddon, J., Seaton, E., and Elfstrom, A. (1999). The amadeus dextrous subsea hand: design, modeling, and sensor processing. *IEEE Journal of Oceanic Engineering*, 24(1):96–111.

Li, M. S., van der Zande, R., Hernndez-Agreda, A., Bongaerts, P., and Stuart, H. S. (2019). Gripper design with rotation-constrained teeth for mobile manipulation of hard, plating corals with human-portable rovs. In *OCEANS 2019 - Marseille*, pages 1–6.

Licht, S., Collins, E., Ballat-Durand, D., and Lopes-Mendes, M. (2016). Universal jamming grippers for deep-sea manipulation. In *OCEANS 2016 MTS/IEEE Monterey*, pages 1–5.

Ludvigsen, M., Søreide, F., Aasly, K., Ellefmo, S., Zylstra, M., and Pardey, M. (2017). ROV based drilling for deep sea mining exploration. In *OCEANS 2017*, pages 1–6, Aberdeen, Scotland.

Mura, D., Barbarossa, M., Dinuzzi, G., Grioli, G., Caiti, A., and Catalano, M. G. (2018). A soft modular end effector for underwater manipulation: A gentle, adaptable grasp for the ocean depths. *IEEE Robotics Automation Magazine*, 25(4):45–56.

Murton, B. J. (2016). JC142 cruise report - marineE-tech project to map the cobalt-rich ferromanganese crust of tropic seamount, NE atlantic ocean. Retrieved November 16, 2018, from https://www.bodc.ac.uk/resources/inventories/cruise_inventory/report/16292/.

Parness, A. (2011). Anchoring foot mechanisms for sampling and mobility in microgravity. In *2011 IEEE International Conference on Robotics and Automation*, pages 6596–6599.

Parness, A., Evans, T., Raff, W., King, J., Carpenter, K., Willig, A., Grimes-York, J., Berg, A., Fouad, E., and Wiltsie, N. (2017a). Maturing microspine grippers for space applications through test campaigns. In *AIAA SPACE and Astronautics Forum and Exposition*, pages 1–17.

Parness, A. and Frost, M. (2012). Microgravity coring: A self-contained anchor and drill for consolidated rock. In *Proceedings of the 2012 IEEE Aerospace Conference*, pages 1–7, Big Sky, MT. IEEE.

Parness, A., Frost, M., Thatte, N., King, J. P., Witkoe, K., Nevarez, M., Garrett, M., Aghazarian, H., and Kennedy, B. (2013). Gravity-independent Rock-climbing Robot and a Sample Acquisition Tool with Microspine Grippers. *Journal of Field Robotics*, 30(6):897–915.

Parness, A., Willig, A., Berg, A., Shekels, M., Arutyunov, V., Dandino, C., and Kennedy, B. (2017b). A microspine tool: Grabbing and anchoring to boulders on the asteroid redirect mission. In *2017 IEEE Aerospace Conference*, pages 1–10.

ROV Manipulator-Based Drilling for Deep Submergence Science (2015). Retrieved November 16, 2018, from https://www.unols.org/sites/default/files/201512desap_23.pdf.

Sager, W., Dick, H., Fryer, P., and Johnson, H. P. (2003). Requirements for robotic underwater drills in us marine geologic research. *JOI/USSAC Newsletter*, 16:12–13.

Sakagami, N., Ishimaru, K., Kawamura, S., Shibata, M., Onishi, H., and Murakami, S. (2013). Development of an underwater robotic inspection system using mechanical contact. *Journal of Field Robotics*, 30(4):624–640.

Stakes, D. S., Holloway, G. L., Tucker, P., Dawe, T. C., et al. (1997). Diamond rotary coring from an rov or submersible for hardrock sample recovery and instrument deployment: The mbari multiple-barrel rock coring system. *Marine Technology Society. Marine Technology Society Journal*, 31(3):11.

Stuart, H., Wang, S., Khatib, O., and Cutkosky, M. R. (2017). The ocean one hands: An adaptive design for robust marine manipulation. *The International Journal of Robotics Research*, 36(2):150–166.

Stuart, H. S., Wang, S., Gardineer, B., Christensen, D. L., Aukes, D. M., and Cutkosky, M. (2014). A compliant underactuated hand with suction flow for underwater mobile manipulation. In *2014 IEEE International Conference on Robotics and Automation (ICRA)*, pages 6691–6697.

TeleRobotics, K. (2005). Predator force feedback manipulator. Retrieved November 1, 2019, from http://krafttelerobotics.com/products/pdfs/predator_pdf.pdf.

Wang, S., Jiang, H., Huh, T. M., Sun, D., Ruotolo, W., Miller, M., Roderick, W. R., Stuart, H. S., and Cutkosky, M. R. (2019). Spinyhand: Contact load sharing for a human-scale climbing robot. *Journal of Mechanisms and Robotics*, 11(3):031009.

YCB Benchmarks Main Page (2016). Retrieved November 16, 2018, from http://ycbbenchmarks.org/.